

http://pubs.acs.org/journal/aesccq Article

# Gas-Particle Uptake and Hygroscopic Growth by Organosulfate Particles

Paul E. Ohno, Junfeng Wang, Fabian Mahrt, Jonathan G. Varelas, Eleonora Aruffo, Jianhuai Ye, Yiming Qin, Kristian J. Kiland, Allan K. Bertram, Regan J. Thomson,\* and Scot T. Martin\*



**Cite This:** *ACS Earth Space Chem.* 2022, 6, 2481–2490



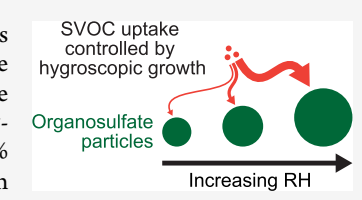
**ACCESS** I

III Metrics & More

Article Recommendations

s) Supporting Information

ABSTRACT: Organosulfate compounds make up a substantial fraction of the particle mass concentration in some regions of the Earth's atmosphere, and organosulfate particles can have sufficiently high viscosity to limit rates of gas-particle interactions. Viscosity varies with relative humidity (RH). Herein, organosulfate particles were exposed to the gas-phase products of  $\alpha$ -pinene photooxidation. The gas-particle partitioning of these species was studied from 15 to 70% RH and <1 to 16 ppb NO at 299 K. The uptake of the  $\alpha$ -pinene oxidation products increased with the increase in RH, and higher gas-phase NO concentrations resulted in increased particle-phase



concentrations of nitrogen compounds. Particle hygroscopicity was examined by optical microscopy. Hygroscopic growth at elevated RH was sufficient to explain the RH-dependent uptake measurements, and kinetic limitations tied to particle viscosity were not observed. The lack of kinetic limitations combined with the Stokes–Einstein equation implied a viscosity much less than  $1 \times 10^6$  Pa s. This value is consistent with estimated viscosities based on literature parameterizations for water mass fractions in the particles of at least 0.05 at 15% RH. Overall, these results suggest that organosulfate hygroscopicity plays a key role in their viscosity and hence in regulating gas-particle partitioning, thereby simplifying the treatment of atmospheric chemistry and transport of pollutants in models of the Earth's atmosphere. The role of organosulfates is expected to take on increasing importance for projected future emission trends.

KEYWORDS: aerosol particles, organosulfates, gas-particle partitioning, hygroscopicity, viscosity, environmental chamber, aerosol mass spectrometry

#### 1. INTRODUCTION

Atmospheric aerosol particles strongly influence climate forcing and human health. 1-3 A substantial mass fraction of atmospheric organic aerosol particles is produced by gas-phase reactions that lead to secondary organic aerosol (SOA).4 Volatile organic compounds (VOCs) emitted from biogenic sources are the predominant global precursor of SOA.<sup>5-7</sup> Interactions between biogenic VOCs and widespread anthropogenic emissions such as nitrogen oxides (NO<sub>x</sub>) and sulfur dioxide (SO<sub>2</sub>) are complex, and in some cases, these anthropogenic emissions can increase the SOA produced from the oxidation of biogenic precursors.8 Specifically, some semi-volatile organic compounds (SVOCs) that otherwise would remain in the gas phase instead undergo uptake into the SOA particles and thereby increase SOA particle mass concentrations. Furthermore, gas-particle partitioning can affect growth rates of the particles, thereby influencing the evolution of the size distribution of atmospheric aerosol particles. Health and climate effects depend strongly on particle size.9,10

Recently, particle-phase organosulfate compounds have gained increased attention in the atmospheric science community. These compounds form upon the mixing of biogenic organic and anthropogenic sulfate emissions, especially in the presence of acidic sulfate particles. The

oxidation products of isoprene, the most abundant non-methane hydrocarbon emitted to the atmosphere, react with sulfuric acid in the condensed phase, and this reaction can appreciably contribute to the accretion of additional organic particle mass. <sup>18–20</sup> The contribution of organosulfates to the total organic particle mass concentration may be as high as 30% at some locations and times. <sup>13</sup> Even as overall global anthropogenic emissions of sulfate are expected to decrease in the future due to a combination of emission controls and the reduction of fossil fuel usage, this decrease is expected to enhance the fraction of atmospheric sulfate that exists as organosulfates. <sup>16,17</sup>

The interactions of organosulfate particles with the gas phase are influenced by their physicochemical properties. <sup>21–25</sup> A key particle property is viscosity, which depends on particle water content and hence relative humidity (RH) due to hygroscopic growth. <sup>26</sup> The uptake of gas-phase species into the organosulfate particles can in turn alter particle physicochem-

Received: June 28, 2022 Revised: September 6, 2022 Accepted: September 7, 2022 Published: September 19, 2022





ical properties, thereby forming a feedback loop that remains incompletely understood. Many experimental and theoretical studies have established that atmospheric organic particles can have viscosities that place a kinetic limit on the rate of gasparticle partitioning. $^{26-31}$ 

In the present study, organosulfate particles are exposed to a gas-phase mixture of the products of  $\alpha$ -pinene photooxidation.  $\alpha$ -Pinene is often co-emitted with isoprene,<sup>32</sup> and the gas-phase oxidation products of  $\alpha$ -pinene can partition to the organosulfate particles. The conducted experiments quantify the RH-dependent uptake of these oxidation products to the organosulfate particles, and in particular, the experiments focus on the impacts of the physicochemical properties of the particles on gas-particle interactions. Two types of organosulfate particles, produced from pure synthesized reference species, were studied (Figure 1). One structure had a primary

#### Organosulfates

**Figure 1.** Organosulfate compounds investigated in this study. (1) Tertiary organosulfate: (2*R*,3*S*)-1,3,4-trihydroxy-2-methylbutan-2-yl sulfate. (2) Primary organosulfate: (2*R*,3*R*)-2,3,4-trihydroxy-2-methylbutyl sulfate. Compounds were prepared as ammonium salts.

carbon with respect to the sulfate moiety, and the other had a tertiary carbon. These two compounds are produced in the atmosphere by reactions of isoprene-derived epoxydiol (IEPOX) with sulfate particles. For the experimental design herein, pure organosulfates are employed to probe the effects of molecular structure on the coupling between physicochemical properties and gas-particle interactions. In the atmosphere, the production of organosulfate particles is dominated by isoprene emissions from the biosphere in the southeastern United States<sup>33,34</sup> and the Amazon basin.<sup>35</sup> These two regions differ, however, in the relative importance of inorganic sulfate, and the experiments herein, which lack inorganic sulfate, represent present-day conditions in the Amazon basin. They are also expected to represent future conditions in the southeastern United States 16 for which inorganic sulfate concentrations continue to decrease in response to the decreasing use of coal in energy production.

#### 2. EXPERIMENTAL SECTION

**2.1. Uptake of SVOC Oxidation Products.** A schematic of the experimental setup for the uptake experiments is shown in Figure 2. The overall apparatus consisted of generation of organosulfate particles, generation of SVOC oxidation products, an exposure chamber where the organosulfate particles were allowed to take up gas-phase oxidation products, and analytical instrumentation for aerosol characterization.

Organosulfate aerosol particles were produced from synthesized compounds, as follows. The synthesized compounds used in the study were the isoprene-derived racemic tertiary sulfate 1 and racemic primary sulfate 2 (Figure 1). Compound purity exceeded >95% based on the <sup>1</sup>H NMR spectra. The synthetic procedures (Section S2) and the NMR spectra (Section S3) appear in the Supporting Information. Aqueous solutions  $(0.3 \text{ g L}^{-1})$  of the compounds were nebulized to produce organosulfate particles. A solution was injected into the nebulizer (Meinhard, TQ+ Quartz Low Internal Volume Nebulizer) by a syringe pump (Chemyx, Fusion 200) at an injection rate of 0.2 mL h<sup>-1</sup>. The nebulizer was supplied with 1 sLpm of zero air from a pure air generator (AADCO Instruments, 737-14A). The produced organosulfate particles were used directly in the uptake experiments. The compounds were not expected to hydrolyze during the course of the experiments based on hydrolysis lifetimes.

SVOC oxidation products were produced by the oxidation of a parent hydrocarbon in the Harvard Environmental Chamber (HEC). A detailed description appeared previously.<sup>37</sup> In brief, the HEC consisted of a 4.7 m<sup>3</sup> PFA bag in a temperature-controlled room. The HEC was operated as a continuously mixed flow reactor at 299  $\pm$  2 K. Inlet flow rates of air, SVOC, H<sub>2</sub>O<sub>2</sub>, and NO were balanced by the exhaust and sampling flow rates. The total flow rate of 21.7 sLpm resulted in a mean residence time of 3.6 h in the chamber. The VOC  $\alpha$ pinene (Sigma-Aldrich, ≥ 98% purity) was injected into a round-bottom flask using a syringe pump at room temperature. A carrier flow swept the  $\alpha$ -pinene vapor into the chamber. The  $\alpha$ -pinene gas-phase concentration in the HEC was 40 ppb prior to the onset of oxidation. As an OH radical precursor, an aqueous solution of H<sub>2</sub>O<sub>2</sub> (50% w/w, Sigma-Aldrich) was injected into a nebulizer (Meinhard) by a syringe pump. The nebulized particles fully evaporated prior to entering the HEC, resulting in a gas-phase H<sub>2</sub>O<sub>2</sub> concentration of 4 ppm. A mass flow controller (Alicat, MC-Series) adjusted the amount of injected nitric oxide (1 ppm in N2, Airgas) to achieve

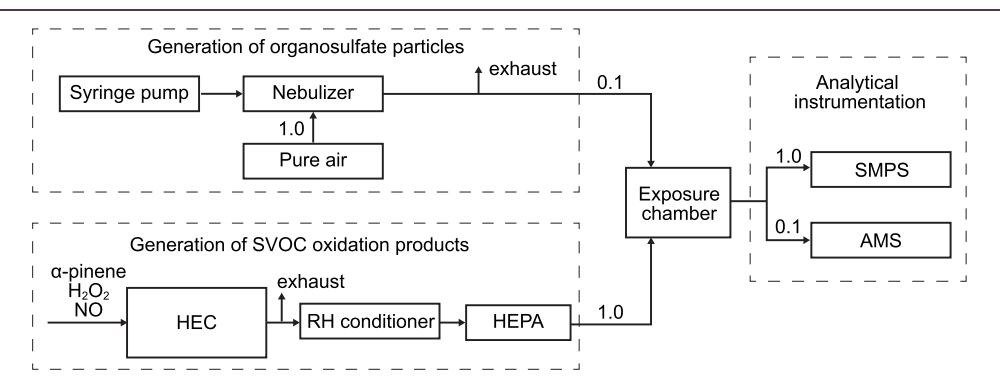


Figure 2. Diagram of the experimental apparatus. Components include the generation of organosulfate particles, generation of SVOC oxidation products, an exposure chamber of particles to oxidation products, and analytical instrumentation of particle chemistry and size distributions. Arrows indicate directions of flows. Numbers indicate flow rates in sLpm. Abbreviations: HEC, Harvard Environmental Chamber; RH, relative humidity; HEPA, high efficiency particulate air filter; AMS, aerosol mass spectrometer; SMPS, scanning mobility particle sizer.

Table 1. Reaction Conditions, Statistics of Particle Size Distributions, and Mass Concentrations for Each Experiment<sup>a</sup>

| experiment | organosulfate | SVOC        | NO conc.<br>[ppb] | RH  | geometric mean number<br>diameter [nm] | geometric standard<br>deviation [nm] | average mass concentration $[\mu g m^{-3}]$ |
|------------|---------------|-------------|-------------------|-----|--|--------------------------------------|---|
| 1          | tertiary      |             | <1                | 70% | $92 \pm 3$                             | $1.95 \pm 0.02$                      | $42 \pm 6$                                  |
| 2          | tertiary      | lpha-pinene | <1                | 70% | $95 \pm 2$                             | $1.96 \pm 0.01$                      | $44 \pm 4$                                  |
| 3          | tertiary      | lpha-pinene | 4                 | 70% | $89 \pm 2$                             | $1.93 \pm 0.02$                      | $37 \pm 4$                                  |
| 4          | tertiary      | lpha-pinene | 8                 | 15% | $88 \pm 1$                             | $1.86 \pm 0.01$                      | $21 \pm 2$                                  |
| 5          | tertiary      | lpha-pinene | 8                 | 40% | $88 \pm 2$                             | $1.86 \pm 0.01$                      | $25 \pm 3$                                  |
| 6          | tertiary      | lpha-pinene | 8                 | 70% | 91 ± 1                                 | $1.85 \pm 0.01$                      | $31 \pm 3$                                  |
| 7          | tertiary      | lpha-pinene | 16                | 70% | $100 \pm 1$                            | $1.83 \pm 0.01$                      | $12 \pm 1$                                  |
| 8          | primary       | lpha-pinene | 8                 | 15% | $72 \pm 2$                             | $1.99 \pm 0.02$                      | $23 \pm 3$                                  |
| 9          | primary       | lpha-pinene | 8                 | 40% | $78 \pm 2$                             | $1.97 \pm 0.02$                      | $24 \pm 4$                                  |
| 10         | primary       | lpha-pinene | 8                 | 70% | $86 \pm 1$                             | $1.97 \pm 0.01$                      | $29 \pm 2$                                  |

<sup>&</sup>quot;Mass concentrations are calculated for a material density of 1.2 g cm<sup>-3</sup> based on the number-diameter distributions. Uncertainty estimates reflect the standard deviation of multiple SMPS scans (10 or more).

concentrations between <1 and 16 ppb in the HEC prior to reaction. The NO concentration reached steady state for at least 24 h prior to the uptake measurements. The NO concentration was measured by a  $NO_x$  analyzer (Thermo-Fisher, 42i-TL). The RH in the HEC was <10% throughout the course of the experiments.

Photooxidation of  $\alpha$ -pinene was initiated by turning on 46 blacklights (Sylvania 350, 40 W) surrounding the bag to photolyze the  $H_2O_2$  and produce OH radicals. The reactions between OH and  $\alpha$ -pinene produced SOA, including both gasphase and particle-phase components. This SOA in the outflow of the chamber subsequently passed through an in-line HEPA filter (Pall, 12144) to remove the particles and lower-volatility oxidation products. Higher-volatility gas-phase oxidation products were retained in the continuing flow.

This flow (1 sLpm) of gas-phase oxidation products was mixed turbulently with a flow (0.1 sLpm) of the organosulfate particles in a downstream exposure chamber (Figure 2). Gasparticle uptake to the particles occurred inside this chamber (7 L, glass). The mean residence time was 380 s. The RH and the temperature before and after the exposure chamber were monitored (Rotronic, HygroClip 2). A custom-built feedback system based on a Nafion humidifier (PermaPure, PD-50T-12SS) controlled the RH of the flow prior to entering the exposure chamber.

Particle chemical composition at the outflow of the exposure chamber was characterized by high-resolution time-of-flight aerosol mass spectrometry (HR-ToF-AMS). AMS data analysis was performed in *Igor Pro* (WaveMetrics Inc.) using the *SQUIRREL* (v1.64) and *PIKA* (v1.24) toolkits. Particle number size distributions were determined by a scanning mobility particle sizer (TSI, SMPS 3080 with CPC 3010), which was operated at an aerosol-to-sheath flow ratio of 5:1. The particle mass concentration was calculated from the particle number-diameter distributions for a material density of 1.2 g cm<sup>-3</sup>. The particle mass concentration was calculated from the particle number-diameter distributions for a material density of 1.2 g cm<sup>-3</sup>. The particle mass concentration was calculated from the particle number-diameter distributions for a material density of 1.2 g cm<sup>-3</sup>.

**2.2.** Hygroscopicity and Contact Angle Measurements. The hygroscopicities of individual, deposited organosulfate particles were characterized by optical and scanning confocal microscopies. The methodology followed previous work. In brief, solutions of approximately 2% (w/w) of each compound were prepared in ultrapure water (Milli-Q, 18.2 M $\Omega$  cm). These solutions were then nebulized (Meinhard, TR-30-C0.5) onto hydrophobically coated glass slides (Cytonix, FluoroPel-800; ORSAtec GmbH, 12 mm diameter). High-purity nitrogen (Linde, 5.0 grade) was used as

a carrier gas. The deposited particles had diameters between 20 and 50  $\mu$ m. The particle-laden hydrophobic glass slides were placed into a temperature and RH-controlled flow cell, which was coupled to an optical microscope (Zeiss, Axiotech, objective lens MAG x20k LD Epiplan, 0.4 aperture). A mixture of dry and humidified flows (1.3 Lpm) of high-purity nitrogen was continuously passed over the particles. The uncertainty in RH was  $\pm 2.5\%$ , as determined by measuring the deliquescence of ammonium sulfate. 42

At the start of each experiment, the particles were equilibrated within the flow cell at close to 100% RH for 5 min. The RH was then continuously decreased to 0%. The RH was changed at rates of 0.1% RH min<sup>-1</sup> from 100 to 75% and 0.5% RH min<sup>-1</sup> from 75 to 0%. Optical images of the particles were recorded using a digital camera (AmScope MU300-HS, 3.1 Aptina Color CMOS) coupled to the microscope. Images at increments of 5 to 10% RH were analyzed in the software *ImageJ* (v 1.53k)<sup>43</sup> to determine the base area *A* of 10 particles at each RH, from which the base radius *r* was calculated by  $r = (A/\pi)^{1/2}$ .

The contact angle  $\theta$  between the particles and the hydrophobic glass slides was measured using a scanning confocal microscope (Zeiss, Axio Observer 510 MP, objective lens MAG x63k Plan-Apochromat, 1.4 aperture), following a method described elsewhere. The measurements were made at approximately 40% RH. The contact angle was measured for 10 individual particles distributed over two independently prepared hydrophobic glass slides for each particle type. The arithmetic mean value of the contact angle for this population of particles is reported. The variability is expressed as twice the standard deviation around the mean.

In respect to calculating particle volume, the particles were taken as spherical caps on the substrate following earlier observations. Spheres of radius R were truncated by the plane of the hydrophobic glass slide. The sphere made a contact angle  $\theta$  with the substrate, resulting in a base radius r given by  $r = R \sin \theta$ . The corresponding spherical cap volume V at a given RH was then calculated as follows:  $^{46}$ 

$$V = \frac{4}{3}\pi R^3 \varphi(\theta) \tag{1}$$

where  $\varphi(\theta)$  is given by

$$\varphi(\theta) = \frac{(2 + \cos \theta)(1 - \cos \theta)^2}{4} \tag{2}$$

The volume growth factor GF at elevated RH was calculated by dividing  $V(\mathrm{RH})$  by V(10%) for each particle: GF =  $V(\mathrm{RH})/V(10\%)$ . The volume at 10% RH was taken as the reference condition because the base area remained unchanged between 10 and 30% RH.

# 3. RESULTS AND DISCUSSION

The conducted uptake experiments are listed in Table 1. Experiment 1 represented a control experiment in which the tertiary organosulfate particles were exposed only to pure air at 70% RH. In experiments 2, 3, 6, and 7, the particles were exposed at 70% RH to the SVOC oxidation products for NO concentrations of <1, 4, 8, and 16 ppb, respectively. In experiments 4, 5, and 6, the tertiary organosulfate particles were exposed at 8 ppb NO to the SVOC oxidation products at 15, 40, and 70% RH, respectively. In experiments 8, 9, and 10, primary organosulfate particles were exposed at 8 ppb NO to the SVOC oxidation products at 15, 40, and 70% RH, respectively. Similar experiments in the HEC observed that the particle-phase yield was highest at 8 ppb for <1 to 16 ppb NO.47 Across the 10 experiments, the geometric mean diameter of the particle population varied from 70 to 100 nm, and the particle mass concentration varied from 10 to 45  $\mu g \text{ m}^{-3}$  (Table 1). The exposure of the organosulfate particles to SVOCs was not observed to substantially increase particle size in the SMPS measurements, as interscan variability during a single experimental condition exceeded differences in size distributions between uptake conditions (Supporting Information, Section S4).

Indicator ions of organic uptake from the gas phase were identified by comparing the mass spectra of the particles in pure air to those of particles exposed to SVOC oxidation products. Supporting Information, Figure S5.1 shows the average mass spectra of the tertiary organosulfate particles at 70% RH exposed only to pure air (experiment 1) and exposed to SVOCs generated with 8 ppb NO at 70% RH (experiment 6). Nitrogen-containing ion fragments were selected as tracer ions for uptake because the organosulfate compounds were free of nitrogen, whereas many of the SVOC oxidation products in the gas phase were organonitrates. Organonitrates also represent a broad class of atmospherically relevant compounds. 48 The chemical composition of organonitrates produced in similar experiments in the HEC was studied by thermal dissociation laser-induced fluorescence, and both peroxy (R-O<sub>2</sub>NO<sub>2</sub>) and alkyl nitrates (R-ONO<sub>2</sub>) were observed. In those experiments, the particle phase was enriched in alkyl nitrates, suggesting that the condensing species were predominantly alkyl nitrates.<sup>47</sup> A caveat, however, is that organosulfate particles were not part of the earlier work, and the dominant condensing species could thus possibly differ in the present study.

Results of experiments 1, 2, 3, 6, and 7 are plotted in Figure 3. In this set of experiments, tertiary organosulfate particles were exposed at 70% RH to SVOC oxidation products produced in the HEC at different injected NO concentrations. In Figure 3a, the ordinate is the ratio of the mass concentration of the  $CH_y^+$  ion family divided by that of the  $SO_4^+$  ion family. The intensities of the  $SO_4^+$  ion family suggest that the organosulfates fragment during electron-impact ionization in the AMS (Figure S5.1), and thus, the intensity of the  $SO_4^+$  ion family is used as a proxy for the organosulfate concentration. Use of the  $CH_y^+$ :  $SO_4^+$  ratio in the analysis removed the effects of small fluctuations in AMS collection efficiency and particle

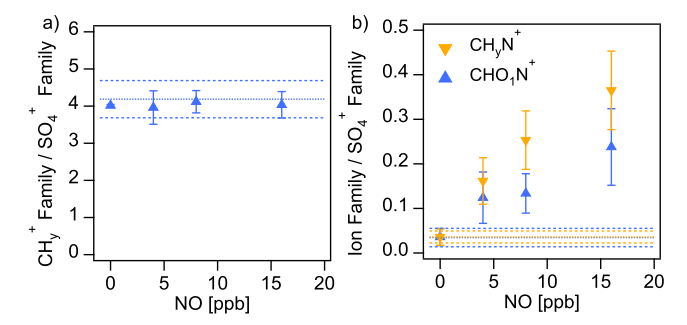


**Figure 3.** Particle composition after exposure to SVOC oxidation products. Results are plotted as a function of the injected NO concentration used in the generation of SVOC oxidation products. (a) Ratio of the mass concentration of the  $CH_y^+$  ion family to that of the  $SO_4^+$  ion family. (b1, orange) Ratio of the mass concentration of the  $CH_yN^+$  ion family to that of the  $SO_4^+$  ion family. (b2, blue) Ratio of the mass concentration of the  $CHO_1N^+$  ion family to that of the  $SO_4^+$  ion family. Conditions: tertiary organosulfate, 70% RH, and 299 K. See also Table 1.

mass concentration during the course of the experiments. In the figure, the dashed-dotted and dashed lines represent the baseline mean and the uncertainty, respectively, for particles exposed to pure air. The absence of a trend in the particlephase  $CH_{\nu}^{+}$  concentration as a function of the gas-phase NO concentration confirmed within experimental uncertainty the expected behavior that the mass concentration of the CH<sub>v</sub><sup>+</sup> ion family arose predominantly from the organosulfate compounds themselves rather than the uptake of SVOC oxidation products. A concern could be that un-photolyzed gas-phase H<sub>2</sub>O<sub>2</sub> partitions into the particles and subsequently reacts to appreciably alter the particle-phase chemistry; however, the similarity of results between experiment 1 (i.e., the control, represented as background lines) and the other experiments in which α-pinene and H<sub>2</sub>O<sub>2</sub> were injected suggests that this phenomenon, if occurring, does not significantly affect the results.

In Figure 3b, the first ordinate is the ratio of the mass concentration of the CH<sub>v</sub>N<sup>+</sup> ion family to that of the SO<sub>4</sub><sup>+</sup> ion family. The ratio of the mass concentration of the CHO<sub>1</sub>N<sup>+</sup> ion family to that of the SO<sub>4</sub><sup>+</sup> ion family is also shown. For <1 ppb NO, the ratios were within baseline uncertainty, as expected. For higher NO concentrations, the ratios increased approximately linearly with NO concentration across the investigated range of <1 to 16 ppb. This trend confirmed that the CH<sub>v</sub>N<sup>+</sup> and CHO<sub>1</sub>N<sup>+</sup> ion families represented the uptake of SVOC oxidation products from the gas phase to the organosulfate particles. Furthermore, the combined evidence of (i) an increase in N-containing fragments for higher NO concentrations and (ii) no changes in particle size distributions across experiments together suggests that the mass fraction of SVOCs in the particles remains small relative to the organosulfate mass. One contributing factor could also be particle-phase reactions of SVOCs that produce highervolatility products that evaporate from the particle phase.

Figure 4 shows the dependence of SVOC oxidation product uptake on RH. Results are shown for both the primary and tertiary organosulfate particles. The ordinate, representing the ratio of the mass concentration of the CH<sub>y</sub>N<sup>+</sup> ion family to that of the SO<sub>4</sub><sup>+</sup> ion family, is scaled in arbitrary units (a.u.) to 1.0 at 15% RH. This scaling allowed relative comparisons between the results for the two particle types. The uptake of SVOC

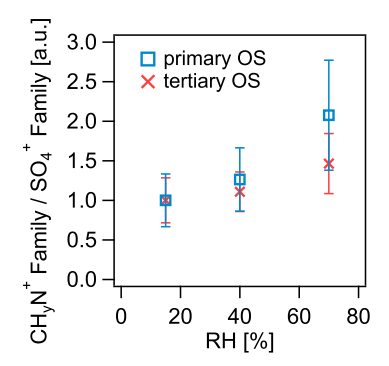


**Figure 4.** Particle composition after exposure to SVOC oxidation products. Results are plotted as a function of the RH inside the exposure chamber. The ratio of the mass concentration of the  $\mathrm{CH}_{\nu}\mathrm{N}^{+}$  ion family to that of the  $\mathrm{SO_4}^{+}$  ion family is plotted. Results are shown for primary and tertiary organosulfate particles. The ordinate is scaled in arbitrary units (a.u.) to 1.0 at 15% RH to allow for relative comparisons between the two organosulfates. Conditions: 8 ppb NO and 299 K. See also Table 1. Abbreviations: RH, relative humidity.

oxidation products, represented by the CH<sub>y</sub>N<sup>+</sup> ion family, increased at higher RH for each organosulfate type.

Hygroscopic particles increase in size at higher RH. The extent of hygroscopic growth of supermicron organosulfate particles was determined by optical microscopy. Shown in Figure 5a,b are representative optical microscopy images of the

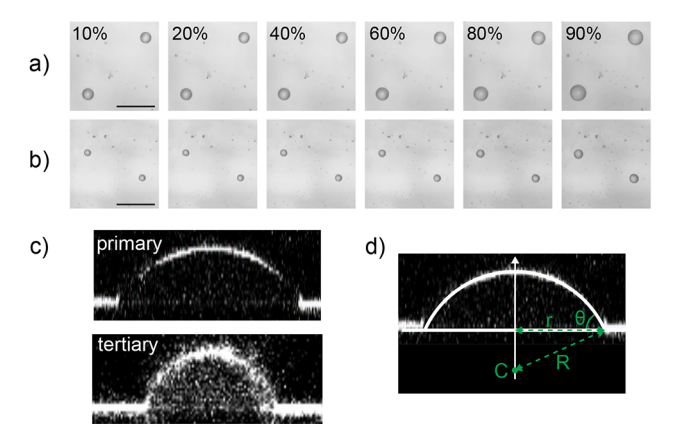


**Figure 5.** Optical microscopy images showing hygroscopic growth for (a) deposited particles of the primary organosulfate and (b) deposited particles of the tertiary organosulfate. Across the series of images RH in the viewing chamber increases from 10 to 90%. There is no exposure to SVOC oxidation products. (c) Confocal images at 40% RH. (d) Geometry of a deposited particle approximated as a spherical cap on a substrate. Terms include sphere radius R, center C, base radius r, and contact angle  $\theta$ . Scale bar = 100  $\mu$ m.

two organosulfate particle types at different RH values. Imaging by confocal microscopy allowed the determination of contact angles of deposited particles (Figure 5c). Contact angles varied from  $58^{\circ}$  to  $73^{\circ}$  for the primary organosulfate (n = 9) and 76 to  $90^{\circ}$  for the tertiary organosulfate (n = 8) where n is the number of particles analyzed. The geometry for determining particle volume V is illustrated in Figure 5d (eqs 1 and 2).

The volume growth factors are plotted as a function of RH in Figure 6. The mean values represent averages over 10 particles of each organosulfate type. The figure shows that the volume growth factors of the primary and tertiary organo-

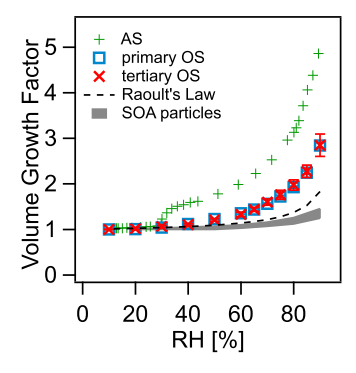


**Figure 6.** Volume growth factor of the organosulfate particles as a function of RH. There is no exposure to SVOC oxidation products. Growth factors are obtained by analysis of the images similar to those shown in Figure 5. Equations 1 and 2 of the main text represent the analysis. Abbreviations: AS, ammonium sulfate; OS, organosulfate; SOA, secondary organic aerosol; RH, relative humidity.

sulfates did not differ from one another across 10 to 90% RH, at least within experimental error. Neither particle type effloresced. The lack of crystallization implies that appreciable amounts of water could remain in the particles even at low RH. Possible changes in surface tension negligibly influenced the hygroscopic growth in these experiments because the particles had supermicron diameters. Differences resulting from the Kelvin effect for atmospheric nanoparticles could still be possible, however. The figure shows that organosulfate hygroscopicity lay between highly hygroscopic inorganic salts such as ammonium sulfate and low hygroscopicity organic materials such as SOA particles produced across a range of oxidation conditions and precursors. Water uptake of the investigated organosulfates also exceeded that predicted for ideal mixing by Raoult's law (cf. Supporting Information).

The increasing uptake of the SVOC oxidation products for increasing RH can arise from a combination of thermodynamic and kinetic factors. As a kinetic influence, higher particle viscosity at lower RH can inhibit the uptake of SVOC oxidation products by slowing particle-phase mass transport (i.e., diffusion). In this case, the surface region of a particle can reach its saturation concentration even as the interior region of the particle remains subsaturated. Such a kinetic inhibition, depressing uptake at low RH, can cause the increase in SVOC uptake at higher RH to exceed the gain in particle-phase volume of hygroscopic growth (i.e., water vapor uptake). The correlation between the volume growth factor and the uptake of SVOC oxidation products is plotted in Figure 7. For both organosulfates, the relationship is linear within the experimental error. The increase in particle volume due to hygroscopic growth thus adequately explains the increase in the uptake of the SVOC oxidation products. The implication is that the uptake reaches thermodynamic equilibrium during the residence time in the exposure chamber. Thermodynamic rather than kinetic factors thus appear to regulate the uptake from 15 to 70% RH at 299 K. Of note, both a single phase or multiple phases (e.g., a core-shell morphology) in thermodynamic equilibrium within the particle is possible, 32 and possible morphologies are not resolved by the conducted experiments.

In the absence of kinetic limitations, two thermodynamic factors can influence and control uptake. First, the concentration of a dissolved gas in the particle phase is proportional to its partial pressure in the gas phase. This partitioning coefficient depends on particle composition (e.g., water

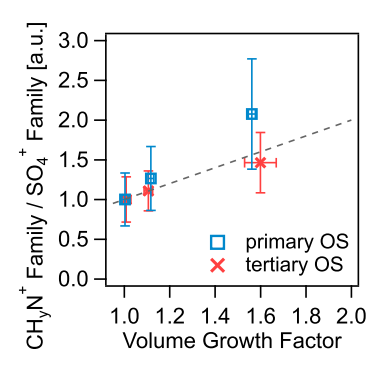


**Figure 7.** Correlation plot between volume growth factor and uptake. Dashed line is a one-to-one line as a guide to the eye. Abbreviations: OS, organosulfate.

content) and thus can change with RH. Second, the uptake mass of SVOC oxidation products per mass of particle sulfate directly scales with particle volume. Particulate sulfate itself is non-volatile. The linear relationship in Figure 7 supports this second interpretation as the primary control of the uptake in the experiments. The uncertainty around the linear relationship, however, is sufficient that a secondary effect of a changing partitioning coefficient might also contribute. The partitioning coefficient could also differ between the two particle types. As a point of comparison, small organic acids can be taken as a firstlevel surrogate of the suite of products from  $\alpha$ -pinene oxidation. 52 The activity coefficients of small organic acids in an organic matrix decrease for increasing water content, implying a change in the partitioning coefficient that favors higher concentrations in the particle phase at higher RH.<sup>24</sup> The possible effects, if present, however, of changing or differing partitioning coefficients, appear minor and lie within the uncertainty of the linear relationship apparent in Figure 7.

In the absence of a kinetic inhibition, an upper limit on the particle viscosity can be estimated. The timescale  $\tau_{\rm mix}$  for diffusion of a molecule throughout a particle of diameter  $d_{\rm p}$  can be estimated as follows<sup>26</sup>

$$\tau_{\text{mix}} = \frac{d_{\text{p}}^2}{4\pi^2 D} \tag{3}$$

for a diffusion constant D. The value of D can be related by the Stokes–Einstein equation to the dynamic viscosity  $\eta$  of the solute for solvent–solute pairs of similar molecular sizes, as follows<sup>26</sup>

$$D = \frac{kT}{6\pi\eta a} \tag{4}$$

for Boltzmann constant k, temperature T, and radius a of the diffusing molecule. A radius a of 4 Å corresponds to typical SOA particle-phase compounds. An exposure time  $\tau_{\rm exp}$  of 380 s pertains to the experiments. For these values and for 90 nm diameter particles (cf. Table 1), a condition of  $\tau_{\rm mix} \ll \tau_{\rm exp}$  (i.e., no kinetic inhibition) requires that  $\eta \ll 1 \times 10^6$  Pa s.

This upper limit implied by the experimental results can be compared to a viscosity that is calculated based on literature parameterizations. The calculation was carried out for 15% RH. This RH was the lowest of the experiments, thus serving as the most stringent test of possible kinetic inhibition (i.e., the calculated viscosity decreases for increasing RH). Furthermore, as an initial case (see case revision further below), water content was taken as negligible at 15% RH based on the

absence of detectable hygroscopic growth between 10 and 30% RH (Figure 6).

The calculation is as follows. The modified Vogel—Tammann–Fulcher equation of a substance such as an anhydrous but non-crystalline organosulfate provides viscosity<sup>54</sup>

$$\eta = \eta_{\infty} \exp\left(\frac{T_0 F}{T - T_0}\right) \tag{5}$$

for viscosity  $\eta_{\infty}$  at infinite temperature and taken as  $10^{-5}$  Pa s herein, <sup>55</sup> fragility parameter F taken as 10, <sup>54</sup> and Vogel temperature  $T_0$ . The value of 10 for the fragility parameter is based on that of other organic compounds of comparable molecular weights, <sup>54</sup> and the sensitivity of the results to this value is analyzed further below. The Vogel temperature is calculated as follows: <sup>55</sup>

$$T_0 = \frac{\beta T_{\rm g}}{F + \beta} \tag{6}$$

for a glass transition temperature  $T_{\rm g}$  and parameter  $\beta$  of 39.17. Two alternative methods of calculating  $T_{\rm g}$  are considered in the analysis. (Method 1) Li et al. <sup>56</sup> presented a parameterization for  $T_g$  based on the vapor pressure and the oxygen-tocarbon atomic ratio of a substance. The vapor pressures of the primary and tertiary organosulfate compounds studied here are estimated in acid form as  $2.42 \times 10^{-8}$  and  $2.07 \times 10^{-8}$  Pa, respectively, by use of COSMOtherm.<sup>57</sup> Resulting  $T_g$  values obtained with these vapor pressures are 319  $\pm$  38 and 320  $\pm$ 38 K for the primary and tertiary compounds, respectively. The uncertainty reflects the accuracy stated by Li et al. (Method 2) The same research group also presented an earlier parameterization based solely on molecular composition (i.e., without vapor pressure).54 Because of the uncertainty in the estimate of the vapor pressure used in method 1, this earlier method is also explored herein. The method incorporates only C, H, and O atoms, so the assumption is made here that an S atom has a quantitatively similar effect on  $T_g$  as an O atom. The resulting  $T_{\rm g}$  of method 2 is 299  $\pm$  21 K for both organosulfate types. Incorporating the lower bounds of these  $T_{\rm g}$  values into eqs 5 and 6 leads to a lower bound of the calculated viscosities of  $\eta > 8.6 \times 10^7$  Pa s for the primary organosulfate and  $\eta > 1.3$  $\times$  10<sup>8</sup> Pa s for the tertiary organosulfate by method 1 and  $\eta$  >  $2.5 \times 10^7$  Pa s for both organosulfates by method 2.

For both methods, the lower bounds of the calculated viscosities exceed the upper limit of the viscosity implied by the experimental observations. Explanations for the mismatch can be considered. The foregoing analysis was based on anhydrous organosulfate. The organosulfate molecules have one sulfate and three hydroxyl moieties (Figure 1), all of which are hygroscopic, and a correction for water content can be considered. As a point of reference, the water mass fraction of aqueous sulfuric acid, which is considered highly hygroscopic, is 0.39 at 15% RH.<sup>59</sup> Water content typically reduces viscosity by acting as a plasticizer in amorphous substances such as SOA particles.<sup>26</sup>

The effect of water content on viscosity can be quantitatively estimated by the Gordon–Taylor equation for  $T_{\rm g,mix}$  of organic-water mixtures at an organic mass fraction  $w_{\rm org}$  (i.e., water mass fraction  $1-w_{\rm org}$ ), as follows:

$$T_{g,mix}(w_{org}) = \frac{(1 - w_{org})T_{g,w} + w_{org}T_{g,org}/\gamma}{(1 - w_{org}) + w_{org}/\gamma}$$
(7)

for a Gordon–Taylor constant  $\gamma$  of 2.5 for organic-water mixtures. The quantity  $T_{\rm g,org}$  of eq 7 corresponds to the quantity  $T_{\rm g}$  of eq 6 calculated by methods 1 or 2. Water mass fractions of 0.05 or greater at 15% RH reconcile the lower bounds of the calculated viscosities with the observed absence of kinetic inhibition in the uptake experiments.

In addition to water as a plasticizer, at least two other nonmutually exclusive possibilities could contribute in part to the overestimation of the calculated viscosity (i.e., higher than that implied by the experimental observations). Regarding a first possibility, a fragility parameter F of 10 was used in eq 5. Although this value is in line with suggestions for SOA particlephase compounds,54 values across a range of organic compounds lie in the range of 5 to 30.61 A fragility parameter of 5 instead of 10 decreases the lower bound of the calculated viscosity sufficiently to eliminate a kinetic inhibition in uptake. Regarding a second possibility, the classic Stokes-Einstein equation can underestimate diffusivity in viscous matrices. 54,56 For these cases, a fractional parameter  $\varepsilon$  has been introduced to match calculated and observed diffusion in SOA mixtures. 6 The value of this parameter is estimated herein as  $\varepsilon = 0.86$ following Evoy et al. 63 for a mean molecular weight of 178 g  $\text{mol}^{-1}$  for the constituents of  $\alpha$ -pinene-derived SOA particles. For this fractional parameter, the modified Stokes-Einstein equation increases by a factor of 30 the upper limit of the viscosity implied by the experiments herein. In short, a fragility parameter less than 5, a fractional Stokes-Einstein parameter less than 0.80, or a water mass fraction greater than 0.05 at 15% RH can separately reconcile the lower bound of the calculated viscosities with the upper limit on viscosity implied by the experimental observations. Combinations of these factors are also possible.

The results of this study can be compared to those of earlier studies. Olson et al. 15 and Riva et al. 16 observed that particle viscosity increased as a consequence of organosulfate production during the uptake of gas-phase epoxydiols to acidified sulfate particles. Zhang et al. 32,58 further found that the uptake became kinetically inhibited as a result of this increase in viscosity. The apparent contradiction with results of the present study can be considered. The organosulfates produced in the previous studies from the reactions of IEPOX with inorganic sulfate resulted in a complex mixture of organosulfates. Monomers, as well as dimers, trimers, and higher-order oligomers, were all produced. 16 These multi-mer species might increase the viscosity and thus introduce kinetic inhibition, unlike the monomers in the present study. Further studies of single-compound organosulfate particles, including such dimers and trimers, are well motivated to further elucidate the molecular basis of the different physicochemical properties of viscosity on gas-particle partitioning.

## 4. CONCLUSIONS

The results presented herein show that the uptake of SVOC oxidation products by primary and tertiary organosulfate particles increases with RH. Furthermore, the hygroscopic growth of the particles explains the increase in uptake at higher RH as a volume-based thermodynamic phenomenon without kinetic inhibition, implying that  $\eta \ll 1 \times 10^6$  Pa s from 15 to 70% RH at 299 K. The important roles of water content and

monomeric organosulfates are the most plausible combined explanation for reconciling the observations herein with earlier laboratory studies and parameterization results. In outlook, emission trends suggest a future atmospheric composition characterized by a greater fraction of organosulfates. <sup>16</sup> The greater hygroscopicity of organosulfate particles compared to other common types of SOA particles suggests that particle hygroscopicity should be increasingly considered in order to mechanistically understand and accurately model gas-particle partitioning and atmospheric composition. Ultimately, further studies of a greater range of organosulfate compounds, including studies on hygroscopic properties and multi-meric species, are motivated to determine the molecular origins of the variability in viscosity of organosulfate particles and the effects that this variability has on gas-particle partitioning.

## DATA AVAILABILITY

The underlying data from the figures can be found at https://doi.org/10.7910/DVN/JZN1SB.

## ASSOCIATED CONTENT

# Supporting Information

The Supporting Information is available free of charge at https://pubs.acs.org/doi/10.1021/acsearthspace-chem.2c00195.

Raoult's Law calculation, summary of synthetic procedures, NMR spectra of synthesized compounds, SMPS size distributions, and average AMS mass spectra (PDF)

# AUTHOR INFORMATION

# **Corresponding Authors**

northwestern.edu

Regan J. Thomson — Department of Chemistry, Northwestern University, Evanston, Illinois 60208, United States; orcid.org/0000-0001-5546-4038; Email: r-thomson@

Scot T. Martin — School of Engineering and Applied Sciences & Department of Earth and Planetary Sciences, Harvard University, Cambridge, Massachusetts 02138, United States; orcid.org/0000-0002-8996-7554; Email: scot\_martin@harvard.edu

## **Authors**

Paul E. Ohno – School of Engineering and Applied Sciences & Department of Earth and Planetary Sciences and Center for the Environment, Harvard University, Cambridge, Massachusetts 02138, United States; orcid.org/0000-0003-4192-1888

Junfeng Wang – School of Engineering and Applied Sciences & Department of Earth and Planetary Sciences, Harvard University, Cambridge, Massachusetts 02138, United States

Fabian Mahrt — Department of Chemistry, University of British Columbia, Vancouver, British Columbia V6T 1Z1, Canada; Laboratory of Environmental Chemistry, Paul Scherrer Institute, Villigen 5232, Switzerland; ◎ orcid.org/0000-0002-7059-6765

Jonathan G. Varelas – Department of Chemistry, Northwestern University, Evanston, Illinois 60208, United States

Eleonora Aruffo — School of Engineering and Applied Sciences & Department of Earth and Planetary Sciences, Harvard University, Cambridge, Massachusetts 02138, United States;

- Department of Advanced Technologies in Medicine & Dentistry, University "G. d'Annunzio" of Chieti-Pescara, Chieti 66100, Italy; orcid.org/0000-0002-9164-7293
- Jianhuai Ye School of Engineering and Applied Sciences & Department of Earth and Planetary Sciences, Harvard University, Cambridge, Massachusetts 02138, United States
- Yiming Qin School of Engineering and Applied Sciences & Department of Earth and Planetary Sciences, Harvard University, Cambridge, Massachusetts 02138, United States
- Kristian J. Kiland Department of Chemistry, University of British Columbia, Vancouver, British Columbia V6T 1Z1, Canada; oorcid.org/0000-0002-4511-8526
- Allan K. Bertram Department of Chemistry, University of British Columbia, Vancouver, British Columbia V6T 1Z1, Canada; o orcid.org/0000-0002-5621-2323

Complete contact information is available at: https://pubs.acs.org/10.1021/acsearthspacechem.2c00195

#### **Notes**

The authors declare no competing financial interest.

#### ACKNOWLEDGMENTS

This work was funded in part by Environmental Chemical Sciences of the Division of Chemistry of the USA National Science Foundation (award numbers 2003368 and 2003359). P.E.O. acknowledges support from the Schmidt Science Fellowship in Partnership with the Rhodes Trust and from the Harvard University Center for the Environment. E.A. and F.M. acknowledge funding from the European Union's Horizon 2020 Research and Innovation Programme under the Marie Skłodowska-Curie Action (840217, E.A.; 890200, F.M.). K.J.K. and A.K.B. acknowledge funding from Natural Sciences and Engineering Research Council of Canada (NSERC) through grant RGPIN/04441-2016.

# REFERENCES

- (1) Fuzzi, S.; Baltensperger, U.; Carslaw, K.; Decesari, S.; Denier van der Gon, H.; Facchini, M. C.; Fowler, D.; Koren, I.; Langford, B.; Lohmann, U.; Nemitz, E.; Pandis, S.; Riipinen, I.; Rudich, Y.; Schaap, M.; Slowik, J. G.; Spracklen, D. V.; Vignati, E.; Wild, M.; Williams, M.; Gilardoni, S. Particulate matter, air quality and climate: lessons learned and future needs. *Atmos. Chem. Phys.* **2015**, *15*, 8217–8299.
- (2) Steiner, A. L. Role of the Terrestrial Biosphere in Atmospheric Chemistry and Climate. *Acc. Chem. Res.* **2020**, *53*, 1260–1268.
- (3) Su, H.; Cheng, Y.; Pöschl, U. New Multiphase Chemical Processes Influencing Atmospheric Aerosols, Air Quality, and Climate in the Anthropocene. *Acc. Chem. Res.* **2020**, *53*, 2034–2043.
- (4) Zhang, Q.; Jimenez, J. L.; Canagaratna, M. R.; Allan, J. D.; Coe, H.; Ulbrich, I.; Alfarra, M. R.; Takami, A.; Middlebrook, A. M.; Sun, Y. L.; Dzepina, K.; Dunlea, E.; Docherty, K.; DeCarlo, P. F.; Salcedo, D.; Onasch, T.; Jayne, J. T.; Miyoshi, T.; Shimono, A.; Hatakeyama, S.; Takegawa, N.; Kondo, Y.; Schneider, J.; Drewnick, F.; Borrmann, S.; Weimer, S.; Demerjian, K.; Williams, P.; Bower, K.; Bahreini, R.; Cottrell, L.; Griffin, R. J.; Rautiainen, J.; Sun, J. Y.; Zhang, Y. M.; Worsnop, D. R. Ubiquity and dominance of oxygenated species in organic aerosols in anthropogenically-influenced Northern Hemisphere midlatitudes. *Geophys. Res. Lett.* 2007, 34, L13801.
- (5) Tsigaridis, K.; Kanakidou, M. Global modelling of secondary organic aerosol in the troposphere: a sensitivity analysis. *Atmos. Chem. Phys.* **2003**, *3*, 1849–1869.
- (6) Hallquist, M.; Wenger, J. C.; Baltensperger, U.; Rudich, Y.; Simpson, D.; Claeys, M.; Dommen, J.; Donahue, N. M.; George, C.; Goldstein, A. H.; Hamilton, J. F.; Herrmann, H.; Hoffmann, T.; Iinuma, Y.; Jang, M.; Jenkin, M. E.; Jimenez, J. L.; Kiendler-Scharr, A.; Maenhaut, W.; McFiggans, G.; Mentel, T. F.; Monod, A.; Prévôt, A. S.

- H.; Seinfeld, J. H.; Surratt, J. D.; Szmigielski, R.; Wildt, J. The formation, properties and impact of secondary organic aerosol: current and emerging issues. *Atmos. Chem. Phys.* **2009**, *9*, 5155–5236.
- (7) Spracklen, D. V.; Jimenez, J. L.; Carslaw, K. S.; Worsnop, D. R.; Evans, M. J.; Mann, G. W.; Zhang, Q.; Canagaratna, M. R.; Allan, J.; Coe, H.; McFiggans, G.; Rap, A.; Forster, P. Aerosol mass spectrometer constraint on the global secondary organic aerosol budget. *Atmos. Chem. Phys.* **2011**, *11*, 12109–12136.
- (8) Shrivastava, M.; Cappa, C. D.; Fan, J.; Goldstein, A. H.; Guenther, A. B.; Jimenez, J. L.; Kuang, C.; Laskin, A.; Martin, S. T.; Ng, N. L.; Petaja, T.; Pierce, J. R.; Rasch, P. J.; Roldin, P.; Seinfeld, J. H.; Shilling, J.; Smith, J. N.; Thornton, J. A.; Volkamer, R.; Wang, J.; Worsnop, D. R.; Zaveri, R. A.; Zelenyuk, A.; Zhang, Q. Recent advances in understanding secondary organic aerosol: Implications for global climate forcing. *Rev. Geophys.* 2017, 55, 509–559.
- (9) Kodros, J. K.; Volckens, J.; Jathar, S. H.; Pierce, J. R. Ambient Particulate Matter Size Distributions Drive Regional and Global Variability in Particle Deposition in the Respiratory Tract. *GeoHealth* **2018**, 2, 298–312.
- (10) Dusek, U.; Frank, G. P.; Hildebrandt, L.; Curtius, J.; Schneider, J.; Walter, S.; Chand, D.; Drewnick, F.; Hings, S.; Jung, D.; Borrmann, S.; Andreae, M. O. Size Matters More Than Chemistry for Cloud-Nucleating Ability of Aerosol Particles. *Science* **2006**, *312*, 1375.
- (11) Surratt, J. D.; Kroll, J. H.; Kleindienst, T. E.; Edney, E. O.; Claeys, M.; Sorooshian, A.; Ng, N. L.; Offenberg, J. H.; Lewandowski, M.; Jaoui, M.; Flagan, R. C.; Seinfeld, J. H. Evidence for Organosulfates in Secondary Organic Aerosol. *Environ. Sci. Technol.* **2007**, *41*, 517–527.
- (12) Iinuma, Y.; Müller, C.; Berndt, T.; Böge, O.; Claeys, M.; Herrmann, H. Evidence for the Existence of Organosulfates from  $\beta$ -Pinene Ozonolysis in Ambient Secondary Organic Aerosol. *Environ. Sci. Technol.* **2007**, *41*, 6678–6683.
- (13) Surratt, J. D.; Gómez-González, Y.; Chan, A. W. H.; Vermeylen, R.; Shahgholi, M.; Kleindienst, T. E.; Edney, E. O.; Offenberg, J. H.; Lewandowski, M.; Jaoui, M.; Maenhaut, W.; Claeys, M.; Flagan, R. C.; Seinfeld, J. H. Organosulfate Formation in Biogenic Secondary Organic Aerosol. *J. Phys. Chem. A* **2008**, *112*, 8345–8378.
- (14) Hatch, L. E.; Creamean, J. M.; Ault, A. P.; Surratt, J. D.; Chan, M. N.; Seinfeld, J. H.; Edgerton, E. S.; Su, Y.; Prather, K. A. Measurements of Isoprene-Derived Organosulfates in Ambient Aerosols by Aerosol Time-of-Flight Mass Spectrometry-Part 2: Temporal Variability and Formation Mechanisms. *Environ. Sci. Technol.* 2011, 45, 8648–8655.
- (15) Olson, N. E.; Lei, Z.; Craig, R. L.; Zhang, Y.; Chen, Y.; Lambe, A. T.; Zhang, Z.; Gold, A.; Surratt, J. D.; Ault, A. P. Reactive Uptake of Isoprene Epoxydiols Increases the Viscosity of the Core of Phase-Separated Aerosol Particles. *ACS Earth Space Chem.* **2019**, *3*, 1402–1414.
- (16) Riva, M.; Chen, Y.; Zhang, Y.; Lei, Z.; Olson, N. E.; Boyer, H. C.; Narayan, S.; Yee, L. D.; Green, H. S.; Cui, T.; Zhang, Z.; Baumann, K.; Fort, M.; Edgerton, E.; Budisulistiorini, S. H.; Rose, C. A.; Ribeiro, I. O.; e Oliveira, R. L.; dos Santos, E. O.; Machado, C. M. D.; Szopa, S.; Zhao, Y.; Alves, E. G.; de Sá, S. S.; Hu, W.; Knipping, E. M.; Shaw, S. L.; Duvoisin Junior, S.; de Souza, R. A. F.; Palm, B. B.; Jimenez, J.-L.; Glasius, M.; Goldstein, A. H.; Pye, H. O. T.; Gold, A.; Turpin, B. J.; Vizuete, W.; Martin, S. T.; Thornton, J. A.; Dutcher, C. S.; Ault, A. P.; Surratt, J. D. Increasing Isoprene Epoxydiol-to-Inorganic Sulfate Aerosol Ratio Results in Extensive Conversion of Inorganic Sulfate to Organosulfur Forms: Implications for Aerosol Physicochemical Properties. *Environ. Sci. Technol.* 2019, 53, 8682–8694.
- (17) Brüggemann, M.; Xu, R.; Tilgner, A.; Kwong, K. C.; Mutzel, A.; Poon, H. Y.; Otto, T.; Schaefer, T.; Poulain, L.; Chan, M. N.; Herrmann, H. Organosulfates in Ambient Aerosol: State of Knowledge and Future Research Directions on Formation, Abundance, Fate, and Importance. *Environ. Sci. Technol.* **2020**, *54*, 3767.
- (18) Froyd, K. D.; Murphy, S. M.; Murphy, D. M.; de Gouw, J. A.; Eddingsaas, N. C.; Wennberg, P. O. Contribution of isoprene-derived

- organosulfates to free tropospheric aerosol mass. *Proc. Natl. Acad. Sci. U.S.A.* **2010**, *107*, 21360–21365.
- (19) Edney, E. O.; Kleindienst, T. E.; Jaoui, M.; Lewandowski, M.; Offenberg, J. H.; Wang, W.; Claeys, M. Formation of 2-methyl tetrols and 2-methylglyceric acid in secondary organic aerosol from laboratory irradiated isoprene/NO<sub>x</sub>/SO<sub>2</sub>/air mixtures and their detection in ambient PM2.5 samples collected in the eastern United States. *Atmos. Environ.* **2005**, *39*, 5281–5289.
- (20) Surratt, J. D.; Lewandowski, M.; Offenberg, J. H.; Jaoui, M.; Kleindienst, T. E.; Edney, E. O.; Seinfeld, J. H. Effect of Acidity on Secondary Organic Aerosol Formation from Isoprene. *Environ. Sci. Technol.* **2007**, *41*, 5363–5369.
- (21) Kuwata, M.; Martin, S. T. Phase of atmospheric secondary organic material affects its reactivity. *Proc. Natl. Acad. Sci. U.S.A.* **2012**, 109, 17354–17359.
- (22) Liu, P.; Li, Y. J.; Wang, Y.; Bateman, A. P.; Zhang, Y.; Gong, Z.; Bertram, A. K.; Martin, S. T. Highly Viscous States Affect the Browning of Atmospheric Organic Particulate Matter. *ACS Cent. Sci.* **2018**, *4*, 207–215.
- (23) Gong, Z.; Han, Y.; Liu, P.; Ye, J.; Keutsch, F. N.; McKinney, K. A.; Martin, S. T. Influence of Particle Physical State on the Uptake of Medium-Sized Organic Molecules. *Environ. Sci. Technol.* **2018**, *52*, 8381–8389.
- (24) Han, Y.; Gong, Z.; Ye, J.; Liu, P.; McKinney, K. A.; Martin, S. T. Quantifying the Role of the Relative Humidity-Dependent Physical State of Organic Particulate Matter in the Uptake of Semivolatile Organic Molecules. *Environ. Sci. Technol.* **2019**, *53*, 13209–13218.
- (25) Qin, Y.; Ye, J.; Ohno, P.; Zhai, J.; Han, Y.; Liu, P.; Wang, J.; Zaveri, R. A.; Martin, S. T. Humidity Dependence of the Condensational Growth of  $\alpha$ -Pinene Secondary Organic Aerosol Particles. *Environ. Sci. Technol.* **2021**, *55*, 14360–14369.
- (26) Reid, J. P.; Bertram, A. K.; Topping, D. O.; Laskin, A.; Martin, S. T.; Petters, M. D.; Pope, F. D.; Rovelli, G. The viscosity of atmospherically relevant organic particles. *Nat. Commun.* **2018**, *9*, 956.
- (27) Virtanen, A.; Joutsensaari, J.; Koop, T.; Kannosto, J.; Yli-Pirilä, P.; Leskinen, J.; Mäkelä, J. M.; Holopainen, J. K.; Pöschl, U.; Kulmala, M.; Worsnop, D. R.; Laaksonen, A. An amorphous solid state of biogenic secondary organic aerosol particles. *Nature* **2010**, *467*, 824.
- (28) Song, M.; Liu, P. F.; Hanna, S. J.; Zaveri, R. A.; Potter, K.; You, Y.; Martin, S. T.; Bertram, A. K. Relative humidity-dependent viscosity of secondary organic material from toluene photo-oxidation and possible implications for organic particulate matter over megacities. *Atmos. Chem. Phys.* **2016**, *16*, 8817–8830.
- (29) Power, R. M.; Simpson, S. H.; Reid, J. P.; Hudson, A. J. The transition from liquid to solid-like behaviour in ultrahigh viscosity aerosol particles. *Chem. Sci.* **2013**, *4*, 2597–2604.
- (30) Booth, A. M.; Murphy, B.; Riipinen, I.; Percival, C. J.; Topping, D. O. Connecting Bulk Viscosity Measurements to Kinetic Limitations on Attaining Equilibrium for a Model Aerosol Composition. *Environ. Sci. Technol.* **2014**, *48*, 9298–9305.
- (31) Gervasi, N. R.; Topping, D. O.; Zuend, A. A predictive group-contribution model for the viscosity of aqueous organic aerosol. *Atmos. Chem. Phys.* **2020**, *20*, 2987–3008.
- (32) Zhang, Y.; Chen, Y.; Lambe, A. T.; Olson, N. E.; Lei, Z.; Craig, R. L.; Zhang, Z.; Gold, A.; Onasch, T. B.; Jayne, J. T.; Worsnop, D. R.; Gaston, C. J.; Thornton, J. A.; Vizuete, W.; Ault, A. P.; Surratt, J. D. Effect of the Aerosol-Phase State on Secondary Organic Aerosol Formation from the Reactive Uptake of Isoprene-Derived Epoxydiols (IEPOX). *Environ. Sci. Technol. Lett.* 2018, 5, 167–174.
- (33) Chan, M. N.; Surratt, J. D.; Claeys, M.; Edgerton, E. S.; Tanner, R. L.; Shaw, S. L.; Zheng, M.; Knipping, E. M.; Eddingsaas, N. C.; Wennberg, P. O.; Seinfeld, J. H. Characterization and Quantification of Isoprene-Derived Epoxydiols in Ambient Aerosol in the Southeastern United States. *Environ. Sci. Technol.* **2010**, *44*, 4590–4596.
- (34) Chen, Y.; Dombek, T.; Hand, J.; Zhang, Z.; Gold, A.; Ault, A. P.; Levine, K. E.; Surratt, J. D. Seasonal Contribution of Isoprene-Derived Organosulfates to Total Water-Soluble Fine Particulate

- Organic Sulfur in the United States. ACS Earth Space Chem. 2021, 5, 2419–2432.
- (35) Glasius, M.; Bering, M. S.; Yee, L. D.; de Sá, S. S.; Isaacman-VanWertz, G.; Wernis, R. A.; Barbosa, H. M. J.; Alexander, M. L.; Palm, B. B.; Hu, W.; Campuzano-Jost, P.; Day, D. A.; Jimenez, J. L.; Shrivastava, M.; Martin, S. T.; Goldstein, A. H. Organosulfates in aerosols downwind of an urban region in central Amazon. *Environmental Science: Processes & Impacts* 2018, 20, 1546–1558.
- (36) Darer, A. I.; Cole-Filipiak, N. C.; O'Connor, A. E.; Elrod, M. J. Formation and Stability of Atmospherically Relevant Isoprene-Derived Organosulfates and Organonitrates. *Environ. Sci. Technol.* **2011**, *45*, 1895–1902.
- (37) Shilling, J. E.; Chen, Q.; King, S. M.; Rosenoern, T.; Kroll, J. H.; Worsnop, D. R.; McKinney, K. A.; Martin, S. T. Particle mass yield in secondary organic aerosol formed by the dark ozonolysis of  $\alpha$ -pinene. *Atmos. Chem. Phys.* **2008**, *8*, 2073–2088.
- (38) Jayne, J. T.; Leard, D. C.; Zhang, X.; Davidovits, P.; Smith, K. A.; Kolb, C. E.; Worsnop, D. R. Development of an Aerosol Mass Spectrometer for Size and Composition Analysis of Submicron Particles. *Aerosol Sci. Technol.* **2000**, *33*, 49–70.
- (39) DeCarlo, P. F.; Kimmel, J. R.; Trimborn, A.; Northway, M. J.; Jayne, J. T.; Aiken, A. C.; Gonin, M.; Fuhrer, K.; Horvath, T.; Docherty, K. S.; Worsnop, D. R.; Jimenez, J. L. Field-Deployable, High-Resolution, Time-of-Flight Aerosol Mass Spectrometer. *Anal. Chem.* **2006**, *78*, 8281–8289.
- (40) Bodsworth, A.; Zobrist, B.; Bertram, A. K. Inhibition of efflorescence in mixed organic-inorganic particles at temperatures less than 250 K. *Phys. Chem. Chem. Phys.* **2010**, *12*, 12259–12266.
- (41) Pant, A.; Parsons, M. T.; Bertram, A. K. Crystallization of Aqueous Ammonium Sulfate Particles Internally Mixed with Soot and Kaolinite: Crystallization Relative Humidities and Nucleation Rates. *J. Phys. Chem. A* **2006**, *110*, 8701–8709.
- (42) Parsons, M. T.; Mak, J.; Lipetz, S. R.; Bertram, A. K. Deliquescence of malonic, succinic, glutaric, and adipic acid particles. *J. Geophys. Res.: Atmos.* **2004**, *109*, D06212.
- (43) Schneider, C. A.; Rasband, W. S.; Eliceiri, K. W. NIH Image to Image]: 25 years of image analysis. *Nat. Methods* **2012**, *9*, 671–675.
- (44) Chesna, J. W.; Wiedmaier, B. F.; Wang, J.; Samara, A.; Leach, R. K.; Her, T.-H.; Smith, S. T. Aerial wetting contact angle measurement using confocal microscopy. *Meas. Sci. Technol.* **2016**, *27*, 125202.
- (45) Ciobanu, V. G.; Marcolli, C.; Krieger, U. K.; Weers, U.; Peter, T. Liquid-Liquid Phase Separation in Mixed Organic/Inorganic Aerosol Particles. *J. Phys. Chem. A* **2009**, *113*, 10966–10978.
- (46) Iwamatsu, M. A generalized Young's equation to bridge a gap between the experimentally measured and the theoretically calculated line tensions. *J. Adhes. Sci. Technol.* **2018**, *32*, 2305–2319.
- (47) Aruffo, E.; Wang, J.; Ye, J.; Ohno, P.; Qin, Y.; Stewart, M.; McKinney, K.; Di Carlo, P.; Martin, S. T. Partitioning of Organonitrates in the Production of Secondary Organic Aerosols from  $\alpha$ -Pinene Photo-Oxidation. *Environ. Sci. Technol.* **2022**, *56*, 5421–5429.
- (48) Lee, B. H.; Mohr, C.; Lopez-Hilfiker, F. D.; Lutz, A.; Hallquist, M.; Lee, L.; Romer, P.; Cohen, R. C.; Iyer, S.; Kurtén, T.; Hu, W.; Day, D. A.; Campuzano-Jost, P.; Jimenez, J. L.; Xu, L.; Ng, N. L.; Guo, H.; Weber, R. J.; Wild, R. J.; Brown, S. S.; Koss, A.; de Gouw, J. d.; Olson, K.; Goldstein, A. H.; Seco, R.; Kim, S.; McAvey, K.; Shepson, P. B.; Starn, T.; Baumann, K.; Edgerton, E. S.; Liu, J.; Shilling, J. E.; Miller, D. O.; Brune, W.; Schobesberger, S.; D'Ambro, E. L.; Thornton, J. A. Highly functionalized organic nitrates in the southeast United States: Contribution to secondary organic aerosol and reactive nitrogen budgets. *Proc. Natl. Acad. Sci. U.S.A.* 2016, 113, 1516–1521
- (49) Liu, Y.; Kuwata, M.; McKinney, K. A.; Martin, S. T. Uptake and release of gaseous species accompanying the reactions of isoprene photo-oxidation products with sulfate particles. *Phys. Chem. Chem. Phys.* **2016**, *18*, 1595–1600.
- (50) Mikhailov, E.; Vlasenko, S.; Martin, S. T.; Koop, T.; Pöschl, U. Amorphous and crystalline aerosol particles interacting with water vapor: conceptual framework and experimental evidence for

- restructuring, phase transitions and kinetic limitations. *Atmos. Chem. Phys.* **2009**, *9*, 9491–9522.
- (51) Varutbangkul, V.; Brechtel, F. J.; Bahreini, R.; Ng, N. L.; Keywood, M. D.; Kroll, J. H.; Flagan, R. C.; Seinfeld, J. H.; Lee, A.; Goldstein, A. H. Hygroscopicity of secondary organic aerosols formed by oxidation of cycloalkenes, monoterpenes, sesquiterpenes, and related compounds. *Atmos. Chem. Phys.* **2006**, *6*, 2367–2388.
- (52) Eddingsaas, N. C.; Loza, C. L.; Yee, L. D.; Chan, M.; Schilling, K. A.; Chhabra, P. S.; Seinfeld, J. H.; Wennberg, P. O. α-pinene photooxidation under controlled chemical conditions Part 2: SOA yield and composition in low- and high-NO<sub>x</sub> environments. *Atmos. Chem. Phys.* **2012**, *12*, 7413–7427.
- (53) Maclean, A. M.; Li, Y.; Crescenzo, G. V.; Smith, N. R.; Karydis, V. A.; Tsimpidi, A. P.; Butenhoff, C. L.; Faiola, C. L.; Lelieveld, J.; Nizkorodov, S. A.; Shiraiwa, M.; Bertram, A. K. Global Distribution of the Phase State and Mixing Times within Secondary Organic Aerosol Particles in the Troposphere Based on Room-Temperature Viscosity Measurements. ACS Earth Space Chem. 2021, 5, 3458–3473.
- (54) DeRieux, W. S. W.; Li, Y.; Lin, P.; Laskin, J.; Laskin, A.; Bertram, A. K.; Nizkorodov, S. A.; Shiraiwa, M. Predicting the glass transition temperature and viscosity of secondary organic material using molecular composition. *Atmos. Chem. Phys.* **2018**, *18*, 6331–6351.
- (55) Angell, C. A. Relaxation in liquids, polymers and plastic crystals strong/fragile patterns and problems. *J. Non-Cryst. Solids* **1991**, 131–133, 13–31.
- (56) Li, Y.; Day, D. A.; Stark, H.; Jimenez, J. L.; Shiraiwa, M. Predictions of the glass transition temperature and viscosity of organic aerosols from volatility distributions. *Atmos. Chem. Phys.* **2020**, 20, 8103–8122.
- (57) Hyttinen, N.; Elm, J.; Malila, J.; Calderón, S. M.; Prisle, N. L. Thermodynamic properties of isoprene- and monoterpene-derived organosulfates estimated with COSMOtherm. Atmos. Chem. Phys. 2020, 20, 5679–5696.
- (58) Zhang, Y.; Chen, Y.; Lei, Z.; Olson, N. E.; Riva, M.; Koss, A. R.; Zhang, Z.; Gold, A.; Jayne, J. T.; Worsnop, D. R.; Onasch, T. B.; Kroll, J. H.; Turpin, B. J.; Ault, A. P.; Surratt, J. D. Joint Impacts of Acidity and Viscosity on the Formation of Secondary Organic Aerosol from Isoprene Epoxydiols (IEPOX) in Phase Separated Particles. ACS Earth Space Chem. 2019, 3, 2646.
- (59) Stokes, R. H.; Robinson, R. Standard Solutions for Humidity Control at 25° C. *Ind. Eng. Chem.* **1949**, *41*, 2013.
- (60) Koop, T.; Bookhold, J.; Shiraiwa, M.; Pöschl, U. Glass transition and phase state of organic compounds: dependency on molecular properties and implications for secondary organic aerosols in the atmosphere. *Phys. Chem. Chem. Phys.* **2011**, *13*, 19238–19255.
- (61) Angell, C. A. Entropy and Fragility in Supercooling Liquids. J. Res. Natl. Inst. Stand. Technol. 1997, 102, 171–185.
- (62) Evoy, E.; Maclean, A. M.; Rovelli, G.; Li, Y.; Tsimpidi, A. P.; Karydis, V. A.; Kamal, S.; Lelieveld, J.; Shiraiwa, M.; Reid, J. P.; Bertram, A. K. Predictions of diffusion rates of large organic molecules in secondary organic aerosols using the Stokes-Einstein and fractional Stokes-Einstein relations. *Atmos. Chem. Phys.* **2019**, *19*, 10073–10085.
- (63) Evoy, E.; Kamal, S.; Patey, G. N.; Martin, S. T.; Bertram, A. K. Unified Description of Diffusion Coefficients from Small to Large Molecules in Organic-Water Mixtures. *J. Phys. Chem. A* **2020**, *124*, 2301.
- (64) King, S. M.; Rosenoern, T.; Shilling, J. E.; Chen, Q.; Martin, S. T. Cloud condensation nucleus activity of secondary organic aerosol particles mixed with sulfate. *Geophys. Res. Lett.* **2007**, *34*, L24806.